

Chapter

Mid-Infrared Spectroscopy and Challenges in Industrial Environment

Chayan Mitra

Abstract

In recent years, Mid-Infrared spectroscopy has garnered lot of attention from researchers and industries due to the availability of industrial grade room temperature Intra-band and Quantum Cascade Lasers. These lasers are repeatable in their performance and along with Near-Infrared Lasers, it has opened the entire Infra-red spectral band for industrial applications. This enabled widespread applications of tunable laser absorption spectroscopy for real-time, in-situ and non-invasive gas sensing. Though several spectroscopy techniques are currently available, Mid-Infrared Absorption Spectroscopy offers us a unique advantage of measurement of trace gas concentrations of few gases which has very weak transitions in Near-Infrared region. The objectives of this chapter are to discuss about the spectroscopy technique commonly used for Mid-Infrared Lasers, a comparative study with other techniques, noise and some challenges remaining for industrial applications.

Keywords: mid-infrared, Quantum Cascade Laser, absorption spectroscopy, near-infrared, spectroscopy

1. Introduction

1.1 General introduction

The Power Generation industry, one of the growth engines for a nation, today face a unique challenge of market volatility and uncertainty. The industry needs to depend on a diverse set of fuel mix and ensure reliable delivery of power while providing asset level visibility (state of asset performance in real-time). It has to provide electricity to over 1 billion people globally for stable growth while ensuring reduced environmental footprint and improved efficiency. The requirement for real-time demand adjustments in response to supply conditions requires integration of real-time measurements, predictability and operational process optimization. This in-turn requires smarter combination of monitoring devices and analytics. The successful transformation depends largely on merger of physical and digital technologies. Real-time, non-invasive and in-situ sensing technologies are the main connects with the network of assets providing powerful data driven insights – a single unified automation architecture for the utility operators and owners.

Apart from air pollution control, emission measurement provides a deeper insight and characterization of a combustion process and control. There are two distinct categories of emission species from a power plant. CO_2 , H_2O , N_2 and O_2 are the major species of emission and are present in percent concentrations, whereas, NO_x , CO , SO_x , Unburned Hydrocarbons (UHC) and Particulate Matters (PMs) constitutes the minor species and are present in parts per million (ppm) concentrations [1, 2]. Nitrogen oxide (NO_x), carbon monoxide (CO) and sulfur oxide (SO_x) the three most important anthropogenic air pollutants are formed during the combustion process in power generation industry (gas fired, coal fired and oil fired). The emission levels from outlet of the treatment systems is important as it outlines few key parameters for selecting flue gas monitoring systems based on the target application: Measurement range, Measurement uncertainty and accuracy, Purpose of measurement and Interfering species.

Spectroscopy-based system is one of the most versatile technologies available for real-time, non-invasive and accurate measurement of trace gases in a combustion environment or a complex gas mixture.

In a spectroscopic measurement system, one down-selects a target molecular transition (based on a “selection” criteria) of the gas species for analyzing the line strength, line shape (and effect of gas temperature and pressure) and estimation of concentration of the species in the gas mixture. Accurate information about the transition will provide users symptoms of any machine/process health issues, possible causes (when evaluated along with operating parameters), possible consequences (impact on service schedules) and possible mitigation methods. Like any measurement system we have the challenge of mitigation of systematic errors (biases) and random errors (white noise). Systematic errors or biases tend to shift the result (the target molecular transition) to one side. This is particularly important as a molecular transition of any gas species is always closely stacked along with the transitions of moisture (a common product from any combustion process). An error in this case will lead to merger of multiple transitions (or targeting a wrong transition!). Proper laser tuning is probably the most critical step in minimizing this error. Random errors are mostly contributed by noise from the detector circuit ($1/f$ noise, generation-recombination noise and Johnson noise), fluctuations in background radiations (above $3 \mu\text{m}$). These errors can be minimized but cannot be avoided.

1.2 Near-infrared absorption spectroscopy and challenges

Near-Infrared (Near-IR) (wavelength range: visible to $\sim 3 \mu\text{m}$) Tunable Diode Laser Absorption Spectroscopy (TDLAS) is a promising technology for real-time trace gas detection without intruding the flow field. This has applications in multiple fields like, environment monitoring, medical diagnostics, defense and law enforcement. TDLAS technique using Near-IR laser at room temperature monitors the overtones of the molecular transitions which have much weaker line strength than the fundamental transitions [3].

Scanned wavelength Direct absorption spectroscopy (DAS) typically involves irradiating the sample with a laser whose wavelength is periodically changed across a fixed range that is larger than the range at which the gas absorbs. The output intensity is measured as a function of wavelength. **Figure 1a**, shows a schematic of DAS. In DAS, the measured output is a dip in intensity at the absorption wavelength of the sample. This becomes difficult for samples with weak absorption lines, or very low gas concentrations (in which the change in fractional absorbance can be as low as 10^{-5}), where one needs to measure a very small change in intensity riding on a large background intensity.

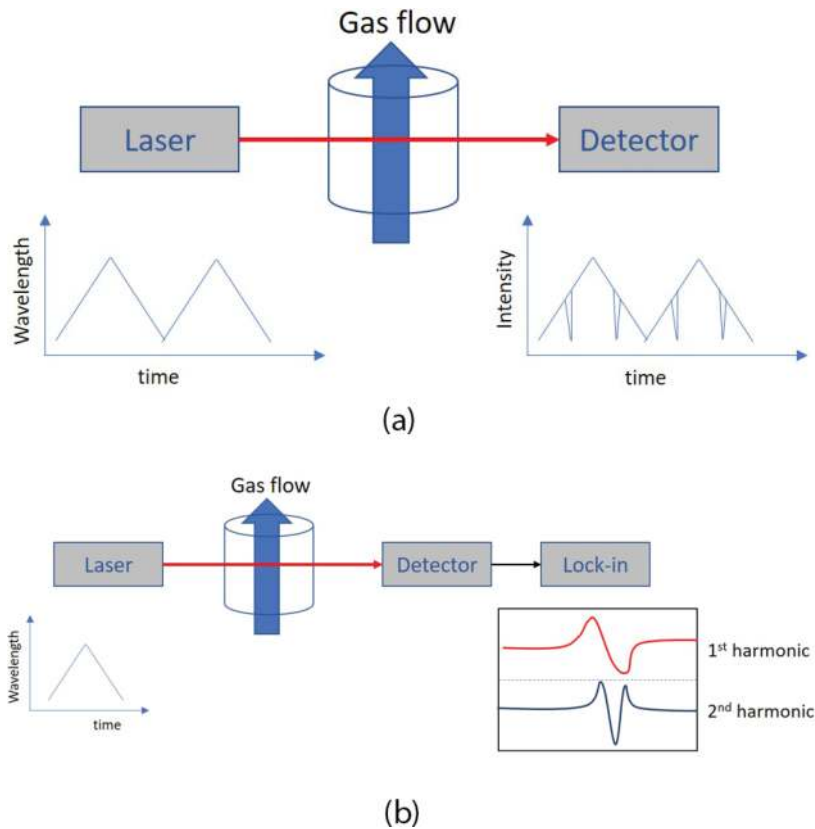


Figure 1. (a) Schematic representation of scanned wavelength direct absorption spectroscopy (DAS). (b) Schematic representation of wavelength modulation spectroscopy (WMS).

Wavelength Modulation Spectroscopy (WMS) or second harmonic detection is a way of increasing the sensitivity of absorption spectroscopy. It involves modulating the laser wavelength and detecting the signal at the second harmonic of the modulation frequency. **Figure 1b** shows a schematic of WMS technique. The benefits of using WMS as opposed to DAS are:

- increased sensitivity,
- insensitivity to interfering species that have broad absorption features in the region of interest,
- Insensitivity to input intensity fluctuations,
- Insensitivity to vibrations.

In WMS, the input wavelength is simultaneously scanned (ramp or triangular waveforms are typically used) and modulated with a sinusoidal waveform. The output intensity is demodulated at the modulation frequency (for first harmonic) and at twice the modulation frequency (for second harmonic). The gas concentration is calculated from the amplitude of the second harmonic signal.

Due to weaker line-strengths and therefore low absorption coefficients of gas species in Near-IR region, absorption spectroscopy in Near-IR has limitations in presence of complex gas mixtures, high pressure and high temperature environment. Availability of industrial grade Interband Cascade Lasers (ICLs) and Quantum Cascade Lasers (QCLs) has enabled application of TDLAS at Mid-Infrared

(Mid-IR) for an accurate and real-time measurement of trace gas content at high temperature in a complex gas mixture environment.

1.3 Enablers of Mid-IR spectroscopy

The first generation QCLs (Quantum Cascade Lasers) operated only in pulsed mode and at ~ 90 K temperature. Significant advancements in epitaxial layer growth processes using Molecular Beam Epitaxy (MBE) and Metallorganic Chemical Vapor Deposition (MOCVD) technologies, bandgap engineering opened the Mid-IR spectral region (wavelength range: 3–24 μm). Subsequently, the continuous single-mode tunability of the QCLs were achieved using tuning schemes like active and simultaneous tuning of grating angles, external cavity length and optical length of the laser chip (drive current tuning and or chip temperature tuning) [4–7].

Gas detection and measurement at trace concentration levels like ppbv (parts per billion in volume) and sub-ppbv or pptv (parts per trillion in volume) requires targeting of strong fundamental roto-vibrational transitions (and hence large absorption coefficient) of the molecules of gas species in the Mid-IR spectral region [8]. Availability of compact, solid-state, high performance and low dissipation single-mode QCLs (Example: Output power 25 mW at 2226 cm^{-1} , dissipated power 1 W [9]) enabled cost-effective usage in several industrial applications without the constraint of heavy packaging in the measurement system. Apart from the QCLs, improvement in detector technology using multi-stage Peltier cooled HgCdTe (Mercury Cadmium Telluride or MCT) Mid-Wavelength Infrared (MWLIR) and Long Wavelength Infrared (LWIR) detectors paved way for stable, fast response (time constant $\tau < 2$ ns [10]) and low noise detection in the entire Mid-IR spectral range (upto $\approx 13\text{ }\mu\text{m}$) [11, 12].

To isolate the QCL devices from any kind of inadvertent exposure to high temperature of the process gas, ease of servicing of the laser modules and ensuring Gaussian beam delivery, Chalcogenide glass (ChGs), Fluoride glass, Sapphire and Silver Halide fibers were initially used for the transmission of Mid-IR lasers as it has wide optical transmission windows in the IR region. A major challenge with the fibers was their brittle nature and laser feedback due to back reflections from the fiber end which reduces signal-to-noise ratio [13, 14]. Last decade has witnessed rapid development of low-loss Hollow Core Waveguides (HCW) for transmission of the Mid-IR beams from the QCLs [15–19]. These are essentially a glass capillary tube with dielectric/metallic structure deposited inside the bore of the tube. Apart from possessing high coupling efficiencies ($>95\%$) and high-power handling capabilities, the hollow core waveguides propagate single-mode [20].

Beam divergence, astigmatism are some of the common challenges one needs to address for all practical applications of Mid-IR spectroscopy [21]. In case of multiple gas species detection, beams from multiple QCL sources are combined along with a red laser (this will be discussed later in Section 4.3). A reflecting beam expander with silver mirror (Wavelength: 450 nm–20 μm , for example *see Thorlabs Product Catalog* [22]) is typically used in these cases. A reflective beam reducing optics is similarly used at the detection end to avoid the chromatic aberrations.

As mentioned previously, the wavelength tuning of QCLs consists of two methods: (1) temperature tuning, (2) injection current tuning. Temperature tuning is slow process and generally used for coarse and slow frequency sweeps [23–25]. Wavelength change through injection current tuning is a much faster process with bandwidth $>100\text{ KHz}$. In this case, the tuning range is much narrower with a significant change in emitted optical power [26, 27]. In modulation spectroscopy techniques, the current modulation sometimes leads to a residual amplitude modulation (RAM) as there is significant change in optical power with injection current.

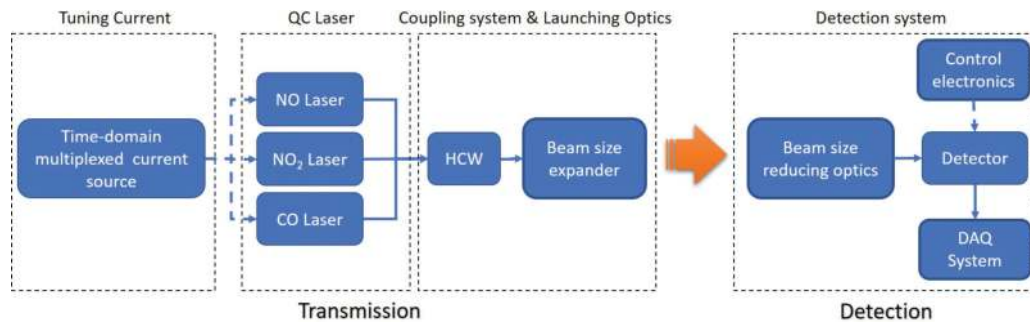


Figure 2. A simplified schematic representation of the Mid-IR spectroscopy system (HCW: hollow core waveguides; DAQ: data acquisition; QC: quantum cascade).

This leads to some distortions in the harmonics of absorption spectra (asymmetry in the $2f$ spectra) [25]. This requires low noise laser current controllers to minimize linewidth, drift and jitter [21, 28]. It should be remembered that commonly used laser diode drivers cannot be used for QCLs due to the compliance voltage which is in the range of 5–15 V.

A simplified schematic of the Mid-IR spectroscopy system is shown in **Figure 2**.

2. Spectroscopy

2.1 Spectroscopic databases and transition lines

As discussed in the introductory section proper down-selection of the roto-vibrational transition lines is a critical part of the process for ensuring accuracy of the measurement system. Several spectroscopic databases, like HITRAN (*High Resolution Transmission*) Molecular Absorption Database [29], HITEMP (*High Temperature Molecular Spectroscopic Database*) [30], GEISA (*Gestion et Etude des Informations Spectroscopiques Atmospheriques*) Spectroscopic Database [31], PNNL (*Pacific Northwest National Laboratory*) Vapor Phase Infrared Spectral Library [32], ATMOS (*Atmospheric Trace Molecule Spectroscopy*) Database [33], NIST (*National Institute of Standards and Technology*) Infrared Spectroscopy Database [34], BT2 (*A high accuracy computed water line list*) Spectroscopic list [35] and CDS (*Carbon Dioxide Spectroscopic Databank*) [36] exists for analyzing the spectroscopic parameters and simulate the transmission spectra. As Mid-IR spectroscopy for industrial applications is the recurrent theme of this chapter, the focus will be on the dominant roto-vibrational transitions in the Mid-IR region for those gas species playing a major role in industrial applications. A summary of rotational-vibration bands and their line-strengths for anthropogenic pollutants NO, NO₂, CO, SO₂ and a major interfering gas (H₂O) in the Mid-IR region is given in **Table 1**.

Table 1 also contains the absorbance values for the gases at temperature (T) = 300 K, Pressure (P) = 1 atm, Length (L) = 100 cm and gas mole-fraction (X) = 1, computed using *SpectraPlot* [41] tool. The line-strength and hence absorbance for H₂O in Mid-IR (ν_1 , ν_2 and ν_3) is almost an order of magnitude higher than in the Near-IR ($\nu_1 + \nu_2$, $\nu_2 + \nu_3$, and $3\nu_2$).

An overview of the roto-vibrational spectra of the above gases in Near-IR and Mid-IR region is shown in **Figure 3**.

It can be noticed that the Mid-IR spectra contains the fundamental vibration modes for H₂O. H₂O has very strong bands in both Near-IR and Mid-IR region and

Gas species	Mode	Wave number (cm ⁻¹)	Line-strength (cm ⁻² /atm)	Absorbance	Ref.
H ₂ O	ν_2	1594.746	1.723×10^{-1}	12	[37, 41]
	$2\nu_2$	3151.629	2.172×10^{-3}	0.18	
	ν_1	3657.629	2.665	1.8×10^2	
	ν_3	3755.928	2.773×10^{-2}	64	
	$3\nu_2$	4666.790	1.961×10^{-2}	0.00013	
	$(\nu_1 + \nu_2)$	5234.976	8.004×10^{-2}	7.0	
	$(\nu_2 + \nu_3)$	5331.267	2.380×10^{-1}	18	
CO	$\Delta\nu = 2 - 1$	2115.625	9.213	4.3×10^3	[38, 41]
	$\Delta\nu = 1 - 0$	2145.999	7.374×10^{-4}	36	
	$\Delta\nu = 3 - 1$	4204.664	3.778×10^{-2}	0.43	
	$\Delta\nu = 2 - 0$	4260.063	2.866×10^{-6}	0.012	
SO ₂	ν_2	517.75	1.635×10^{-2}	45	[38, 39, 41]
	ν_1	1155.920	1.033×10^{-1}	98	
	ν_3	1360.791	5.119×10^{-1}	2×10^3	
	$(\nu_1 + \nu_2 + \nu_3) - \nu_2$	2492.444	2.019×10^{-2}	27	
	$(\nu_1 + \nu_3)$	2498.444	1.334×10^{-2}	38	
NO ₂	ν_2	741.599	7.862×10^{-3}	28	[38, 41]
	$2\nu_2$	1490.77	1.430×10^{-4}	0.35	
	ν_3	1616.152	9.861×10^{-1}	2.4×10^3	
	$(\nu_2 + \nu_3) - \nu_2$	1605.497	2.478	3.8×10^3	
	$\nu_1 + 2\nu_2$	2805.512	7.041×10^{-6}	0.0089	
	$(\nu_1 + \nu_2 + \nu_3) - \nu_2$	2898.193	8.516×10^{-2}	1.5×10^2	
	$\nu_1 + \nu_3$	2906.069	4.967×10^{-2}	89	
NO	$\Delta\nu = 1 - 0$	(1875.959)	3.179×10^{-2}	2.7×10^2	[40, 41]
	$\Delta\nu = 2 - 1$	1875.898	1.908×10^{-2}	5.0×10^2	
	$\Delta\nu = 2 - 0$	3723.526	2.476×10^{-3}	6.1	
	$\Delta\nu = 1 - 0$	1678.184	1.207×10^{-5}	0.00028	
	$\Delta\nu = 2 - 1$	(1846.568)	4.177×10^{-1}	1.3×10^3	

Table 1.

Summary of some major roto-vibrational spectra for anthropogenic pollutants in Mid-IR spectral region.

careful line selection strategy needs to be adopted for accurate spectral analysis of the target gases.

2.2 Selection of transitions

The study of the spectroscopic properties and down-selection of proper transition for the target gas species is extremely important as the sensitivity and accuracy of the gas species measurement in a gas sensor depends primarily on the line selection process. It is the first step towards designing an accurate sensor. The basic criteria for the selection of a transition are existence of strong absorbance and minimal spectral interference from other combustion products (like water vapor). For example, consider the NO₂ transitions in **Table 1**. The transitions at around

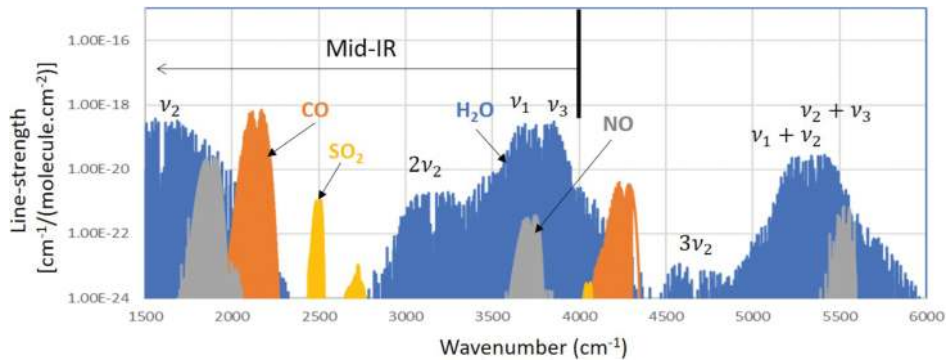


Figure 3. Roto-vibrational spectra of H_2O , NO , CO and SO_2 in NIR and Mid-IR region simulated using spectral data from HITRAN database [29].

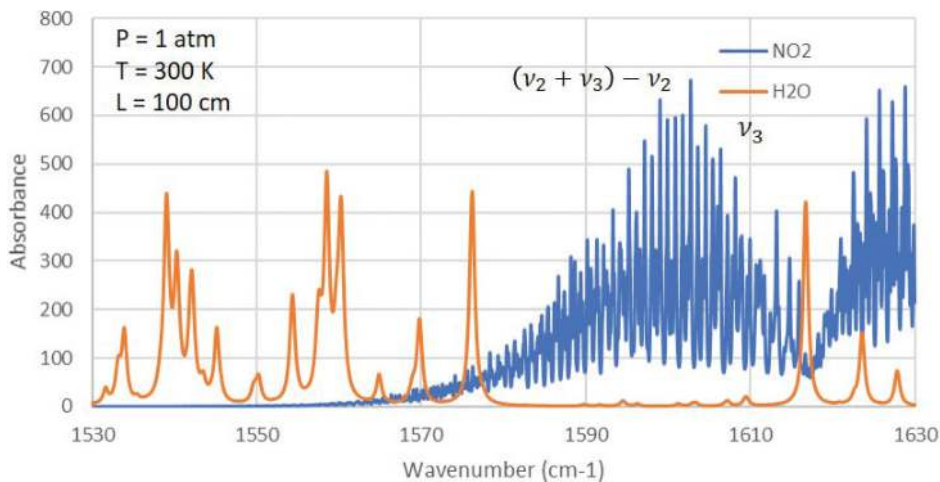


Figure 4. Roto-vibrational spectra of H_2O and NO_2 in Mid-IR region simulated using spectral data from HITRAN database and SpectraPlot tool.

1600 cm^{-1} are the strongest among all the transitions highlighted for NO_2 . In most industrial applications, water vapor is the major interfering species. A simulation study using *SpectraPlot* [41] tool for NO_2 (mole-fraction = 0.1) and H_2O (mole-fraction = 0.8) is shown in **Figure 4**.

Figure 4 shows strong absorption band of NO_2 in 1600 cm^{-1} region with a well-defined and less-structured water vapor spectrum. This is particularly important as it allows the use of wavelength modulation spectroscopy technique to properly differentiate the spectral features of NO_2 and H_2O completely removing the interferences.

2.3 Absorption spectroscopy: basics and models

The theory of laser absorption spectroscopy has been widely discussed in several literatures in details [42–44]. Some of the key equations will be highlighted here to set the stage for further discussions.

The basic equation relating the incident laser intensity and transmitted laser intensity through a gas medium is given by Beer-Lambert's law

$$\left(I_T / I_0 \right)_\nu = \exp(-\alpha_\nu L) \quad (1)$$

Here α_ν denotes the spectral absorbance (also given in **Table 1**) at frequency ν (cm^{-1}). It can also be written as

$$\alpha_\nu = \frac{1}{L} \log \left(I_0 / I_T \right)_\nu = \sum_j P n x_{abs} S_j(T) \phi(\nu, T, P, x_{abs})_j L \quad (2)$$

The spectral absorbance depends on specific gas properties like mole-fraction (x_{abs}), number density of gas (n) in ($\text{molecules}/\text{cm}^3$), line-strength ($S_j(T)$) and line-shape function $\phi(\nu, T, P, x_{abs})_j$ for a specific quantum transition j . The path-length of the laser (interaction length of the laser through the gas sample) is L (cm). In the above equation, T and P are temperature (K) and pressure (atm) respectively. The transition line-shape function is a key parameter which depends on the ν, T, P and the x_{abs} . Various factors like limited lifetime of the energy levels involved in the transition, thermal motion of the molecules broaden the absorption lines and results in a statistical distribution of frequencies around a center frequency of the transition (ν_0). These line-shape functions are mostly symmetric in nature except for those in complex systems (large molecules) [45]. **Table 2** gives the summary of different line-shape models used in absorption spectroscopy (irrespective of whether it is Near-IR or Mid-IR).

From **Table 2**, we can see that the Doppler broadening has strong ν dependence and weak T (temperature) and m (molecular weight of the gas species) dependence. On the other hand, the Lorentzian profile changes with the life-time of the transition state. Doppler broadening is the dominant factor at low pressure and pressure induced shift (Δ) dominates at higher pressure. Apart from the usual Gaussian, Lorentzian and Voigt distributions (which are symmetric distributions), an Asymmetric model is also highlighted in the table. In a multi-peak fitting scenario, degree of overlap, number of non-resolved bands in the profile under study and base-line position are the critical parameters which drives the accuracy of curve fits [47, 48].

The models are developed to provide a ‘best fit’ to the experimental data and to quantify the parameters of interest as described in **Table 2**. Derived using theoretical equations, the parameters provide us specific physical interpretation of the underlying process. The ‘Sum of Squared Residuals’ (Sum of Squared Residuals: square of the difference between a model estimate and the corresponding data point) is often used for estimating the measurement error [49]. At very low-

	Lineshape model	FWHM, Parameters	Mechanism and Ref.
Gaussian	$G(\nu) = \frac{A}{\gamma_0} \sqrt{\frac{4 \ln 2}{\pi}} \exp \left[-4 \ln 2 \left(\frac{\nu - \nu_0}{\gamma_0} \right)^2 \right]$	$\gamma_0 = 2\nu_0 \sqrt{\frac{2 \ln 2 k_B T}{m c^2}}$ γ_0	Doppler broadening [45]
Lorentz	$L(\nu) = \frac{2A/\pi\gamma_L}{1+4[(\nu-\nu_0-\Delta)/\gamma_L]^2}$	$\gamma_L = 1/(4\pi\tau)$ γ_L, Δ	Radiation damping, collision broadening [45]
Pseudo-voigt	$V(\nu) = L(\nu) \otimes G(\nu)$ $V(\nu - \nu_0) = \int_{-\infty}^{\infty} G(\nu' - \nu_0) L(\nu - \nu') d\nu'$	Parameters: $\gamma_0, \gamma_L, \Delta$	Convolution of Gaussian & Lorentzian [45, 46]
Asymmetry	$A(\nu) = \frac{2\gamma_0}{1+\exp[a(\nu-\nu_0)]}$	$a < 0, \nu_0 \rightarrow$ higher wavenumbers $a > 0, \nu_0 \rightarrow$ lower wavenumbers	Complex molecules in Mid-IR [45]

FWHM: full width at half maximum.

Table 2.

Summary of line-shape models used for spectral analysis in absorption spectroscopy along with the parameters characterizing the profiles.

pressure regime (<20 Pa), the Voigt distribution fit of the profile does not reproduce accurately the observed spectral line shape of the gas species. ‘W-shaped’ residuals have been observed in these cases [50]. Galatry profiles (for soft collisions) and Rautian profiles (for hard collisions) have been developed to minimize the observed residuals [51, 52].

The ‘fit’ of the models to the experimental data becomes extremely critical when we try to estimate the gas concentration with ppbv (parts per billion in volume) or pptv (parts per trillion in volume) accuracy levels (in 3σ scales). This will be discussed in detail in Section 3.

2.4 Absorption spectroscopy: effect of temperature

In most real-world applications, it is desirable to measure the gas species concentration at elevated temperatures. Temperature dependency of line-strength and line-shape leads to complications in species concentration estimation in combustion gas flow field. A thorough understanding of ‘fit’ of the models (described in Section 2.3) with the acquired spectra at higher temperatures is important, as it lowers the accuracy levels of the species concentrations.

The temperature dependency of line-strength of a transition is given by Eq. (3):

$$S(T) = S(T_0) \frac{Q(T_0)T_0}{Q(T)T} \left[1 - \exp\left(\frac{hc\nu_0}{k_B T}\right) \right] \left[1 - \exp\left(\frac{hc\nu_0}{k_B T}\right) \right]^{-1} \exp\left[\frac{-hcE''}{k_B} \left(\frac{1}{T} - \frac{1}{T_0}\right)\right] \quad (3)$$

where k_B (Boltzman’s constant), c (speed of light), h (Plank’s constant) are the constant terms and ν_0 is the line-center frequency, E'' is the lower energy state and Q is the partition function. Eq. (3) is given in terms of reference temperature T_0 (296 K) [41, 53].

The accuracy of line-strength and absorbance depends on the accurate knowledge of high temperature partition function $Q(T)$ as shown in Eq. (3). HITEMP database [30] has been developed (based on direct numerical diagonalization, wave function and electric dipole-moment function calculations) to estimate the line-strengths of five species H_2O , CO_2 , CO , NO and OH . A summary of absorbances of H_2O , CO , NO and NO_2 at elevated temperatures are given in **Table 3**.

The condition at 900 K is the typical case one would likely get in a combustion environment. The absorbances for H_2O , CO and NO has been estimated using HITEMP 2010 and *Spectraplot* tool [30, 41]. Absorbance for NO_2 has been estimated using HITRAN 2012 and *Spectraplot* [41, 55]. An experimental determination of broadening parameters γ_0 and temperature-dependent exponent, n , for NO_2 - N_2 and NO_2 -Ar has been discussed in detail in Ref. [54]. The broadening coefficients and the temperature dependent exponent for NO_2 depends on the species it collides with. In the case of the collision partner, lighter the molecule larger the optical collision diameter and *vice-versa*. The wavenumbers were selected based on the availability of lasers and detectors from different suppliers.

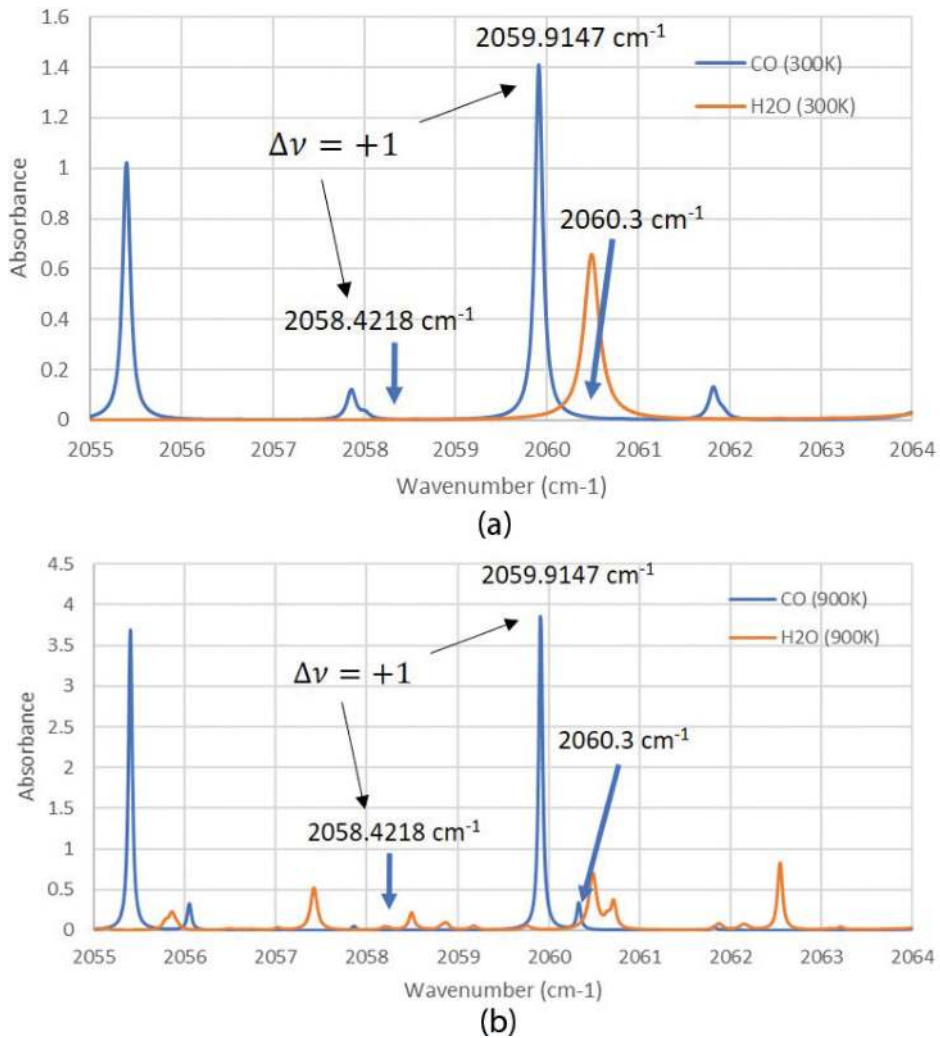
A HITRAN simulation of CO line at two different temperatures (300 and 900 K) for 2059.91 cm^{-1} ($E'' = 806.4\text{ cm}^{-1}$) line using *Spectraplot* tool is given in **Figure 4**.

From **Figure 5**, we can see that at 300 K, the CO transition lines at 2058.4 cm^{-1} (corresponding to $\Delta\nu = +1$) and 2060.3 cm^{-1} are not at all visible [56]. There is a single well-defined water transition at 2060.5 cm^{-1} . The leading edge of the water line overlaps with the trailing edge of the CO line. At 900 K, the line-width of the CO line decrease with an increased absorbance with an appearance of a smaller and well-resolved transition at 2060.3 cm^{-1} ($E'' = 2543.1\text{ cm}^{-1}$). The similar effect is also seen for the water transition line at 2060.5 cm^{-1} .

Gas species	Frequency (cm ⁻¹)	Line strength (cm ⁻² /Atm)	Absorbance			References
			300 K	600 K	900 K	
H ₂ O	2060.48	8.272 × 10 ⁻⁴	0.65	0.94	0.7	HITEMP 2010, SpectraPlot [30, 41]
CO	2013.35	1.118 × 10 ⁻⁵	0.02	0.62	1.20	
	2059.91	8.753 × 10 ⁻⁴	1.4	3.6	3.7	
NO	1927.27	1.183 × 10 ⁻⁴	1.0	1.3	1.0	
	1929.03	1.828 × 10 ⁻⁴	1.6	1.7	1.2	
NO ₂	1599.01	2.324 × 10 ⁻³	16	6	2.3	HITRAN 2012, SpectraPlot [29, 41, 54, 55]
	1599.91	2.802 × 10 ⁻³	15	5	1.8	
	1600.08	1.014 × 10 ⁻⁵		2	0.77	

Table 3.

Variation of absorbance at different temperatures with conditions as mole-fractions ($x_{\text{Gas}} = 0.001$, $x_{\text{H}_2\text{O}} = 0.08$), path-length (L) = 250 cm, pressure (P) = 1 atm, balance N₂.


Figure 5.

(a) HITRAN simulation using Spectraplot tool of a CO and a water transition line at 300 K, (b) HITRAN simulation using Spectraplot tool of a CO and a water transition line at 900 K.

Considering the two transitions at 2059.91 and 2060.3 cm^{-1} , we can infer the gas temperature from the ratio of absorbances at both the transitions of CO. The ratio of absorbances is shown in Eq. (4):

$$\left(\frac{\alpha_{\nu 1}}{\alpha_{\nu 2}}\right) = \frac{S_A(T) \phi(\nu_1, T, P, x_{abs})}{S_B(T) \phi(\nu_2, T, P, x_{abs})} = R(T) \quad (4)$$

The temperature sensitivity is given by

$$\left|\frac{dR/R}{dT/T}\right| \approx \left(\frac{hc}{k_B}\right) \left|\frac{E''_{\nu 1} - E''_{\nu 2}}{T}\right| \quad (5)$$

The $E''_{\nu 1}$ and $E''_{\nu 2}$ are the lower energy states of the two transitions of the CO lines as indicated in **Figure 5(b)**. The sensitivity depends strongly on the difference in the lower energy states of the transitions. A detailed analysis on this is given in the Refs. [57, 58] by Spearrin et al. and Zhou et al. respectively.

2.5 Absorption spectroscopy: techniques

Two categories of laser-based absorption techniques are available for measurement of trace gas species concentration: direct absorption spectroscopy (DAS) and wavelength modulation spectroscopy (WMS). These techniques are further subdivided into two categories based on fixed wavelength and scanned wavelength techniques. Though these techniques were initially developed for spectroscopy in the Near-IR spectral region, it has found widespread application in Mid-IR spectroscopy.

2.5.1 Direct absorption spectroscopy

In direct absorption spectroscopy, the laser wavelength is tuned such that it is resonant with the absorption transition of interest of the gas species. Fixed wavelength direct absorption spectroscopy is rarely used as it contains very limited spectral information and non-absorbing losses (scattering, vibrations, beam-steering) are negligible. In case of scanned-wavelength direct absorption spectroscopy (SW-DAS), the laser injection current is tuned to scan across an absorption transition of interest and the trace gas species properties are estimated using Eq. (2). In this case, the laser frequency tuning range is $\approx 0.1\text{--}10 \text{ cm}^{-1}$. *Hyperspectral direct-absorption spectroscopy* techniques exist for range greater than 10 cm^{-1} .

2.5.2 Wavelength modulation spectroscopy

In a complex gas mixture, like in case of combustion gas or in natural gas, one of the major challenge is to identify an absorption line of the trace gas species isolated from background gases. Also, at elevated temperature, the Boltzmann distribution results in redistribution of molecules among energy states thereby increasing the relative strength of absorption of the far wings of the fundamental bands. This increases the chances of overlap of the trace gas spectra with the background gases. To address this challenge, Wavelength Modulation Spectroscopy (WMS) technique of detection of trace gas has been developed to estimate the concentration in presence of complex background gas mixtures (e.g. CO₂, H₂O, Hydrocarbons).

Several literatures exist discussing the details of the WMS technique [42, 43, 53]. In brief, the harmonics (nf or n^{th} -derivative) of the wavelength modulation

provides several answers to the absorption spectra of the trace gas. The second-harmonic (WMS-2f) is used for trace gas species concentration estimation when the absorbance is quite low. In WMS-2f/1f technique, the WMS-2f signal is normalized with the 1f signal to minimize the non-absorption losses like, beam-steering, scattering, window fouling. This is particularly useful in using the laser-based technique for a robust trace gas species measurement in an industrial environment.

In fixed-WMS, the injection current modulation is used to modulate the laser's wavelength on an absorption transition of interest. Whereas, in case of scanned-WMS, the laser's wavelength modulation is accompanied by a minor amplitude wavelength scan to resolve the peak of the WMS-2f signal normalized with 1f.

Optimization of the modulation depth parameter (a_m) is a critical requirement for an enhanced signal-to-noise ratio (SNR) of the measurement system. The modulation depth parameter is defined in Eqs. (6), (7) as:

$$\nu(t) = \bar{\nu} + \nu_m(t) + \nu_s(t) \quad (6)$$

$$\nu(t) = \bar{\nu} + a_m \cos(2\pi f_m t + \varphi_m) + a_s(2\pi f_s t + \varphi_s) \quad (7)$$

In WMS model, the tuning frequency is a superposition of laser scanning and modulation terms around a mean optical frequency ($\bar{\nu}$). This is a combination of high-frequency modulation (f_m) and a low frequency scan (f_s). In the above equation, a_m (cm^{-1}) and a_s (cm^{-1}) are the modulation depth and scan depth respectively. φ_m and φ_s are the temporal phases of optical frequency tuning [54]. The 2f signal increases with increase in modulation depth and slowly starts to saturate [59]. The initial point of the saturation is considered as the optimal modulation depth for the measurement process. The optimal modulation depth varies with different trace gas species.

2.6 Absorption spectroscopy in Mid-IR

Wavelength modulation Spectroscopy scheme discussed above is widely used in Mid-IR region. The suitability and subsequent modification of the technique depends largely on the knowledge of spectral features of the target gas and its variations with local operating conditions. In Mid-IR region, the transitions of single gas species are sometimes severely convoluted. This requires characterizations of all the components of transition parameters for accurately modeling the profiles [54].

This becomes further complicated during the detection of trace gas in presence of strong spectral interference from species like water. In these cases, one also must consider the effect on sensitivity of the WMS-2f signal due to fluctuations in interference by the interfering species. An optimization method to be used in this case has been discussed in detail by Sur et al. in Ref. [54].

3. Measurement challenges in Mid-IR

For any measurement system, noise, repeatability and reproducibility plays an important role in determining three critical points: (1) factors influencing the measurement process, (2) whether measurement system variability is small compared to process variability and (3) the capability of measurement system to distinguish between parts (or *part-to-part* variation). "*Part-to-part*" variation in the present case will be variations in industrial processes. For any laser-based measurement system, noise and repeatability are the major contributors of measurement errors.

Reproducibility is the variability in measurement system due to differences in operators and cannot be considered in this case.

The availability of industrial grade QCLs for trace gas measurement has enabled sub-ppm and sub-ppb level measurement. The measurement error due to noise and repeatability play an extremely crucial role as we go down to the low concentration and high specificity measurement regime. Various factors like, $1/f$ -noise, pressure (P) and temperature (T) effects, etalon effect contribute to the measurement system noise. Wavelength stability of successive scans leads to short- and long-term drifts in measurement which is mostly a repeatability challenge with the system.

3.1 Noise

In Direct Absorption Spectroscopy (DAS) technique, the noise is usually dominated by $1/f$ -noise of the laser source. This limits the lowest detectable limit to a higher value. Development of high frequency modulation techniques, substantially reduced the $1/f$ -noise in the TDLAS technique. This was further improved by using Mid-IR spectral region for measurement purpose.

Figure 6 gives an overview of the noise regimes and the contributing factors in a laser-based technique.

As discussed above, the $1/f$ -noise is the primary contributor in Section 1, due to the laser source. In Section 2, the gas pressure and temperature are the major factors contributing the deviations from Voigt-only distribution fit (giving the distinct “W-shape” residuals for the best fit) [60].

The detection limit of a trace gas species is calculated as [61, 62],

$$\Delta x_{species} = \frac{\Delta V_{residual}}{V_{Peak}(\nu_0)} \quad (8)$$

In the above equation, $\Delta V_{residual}$ corresponds to the 3σ of the fit residual and $V_{Peak}(\nu_0)$ corresponds to the peak absorption of the Voigt distribution fit at ν_0 . This can be further reduced by averaging over N samples as [63]:

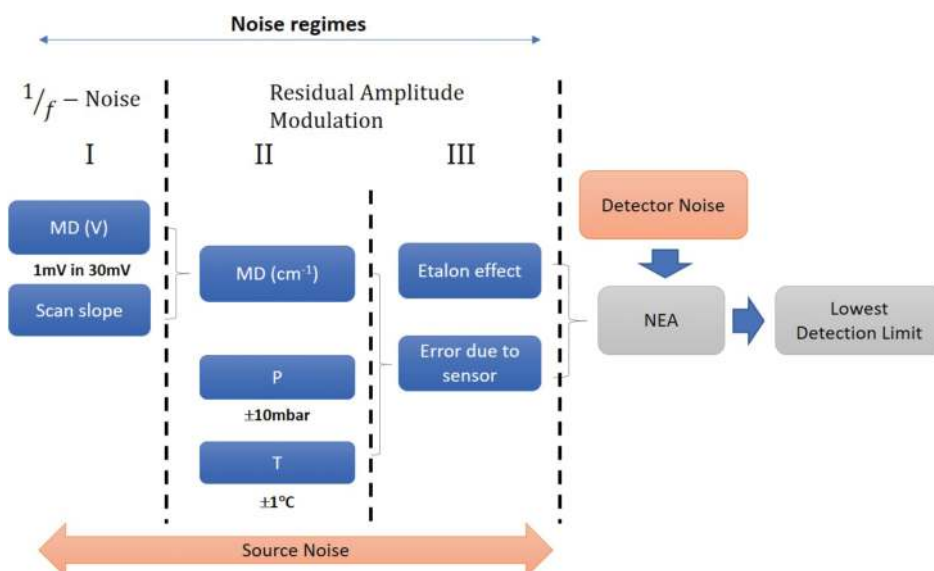


Figure 6. Noise regimes at various sections of the measurement system and the contributing factors to the overall error budget.

$$\langle \Delta V_{residual} \rangle = \frac{1}{N} \sqrt{(\Delta V_{residual})^2} \quad (9)$$

$$\langle \Delta x_{species} \rangle = \frac{\langle \Delta V_{residual} \rangle}{V_{Peak}(\nu_0)} \quad (10)$$

Another important contributor of the noise are the Etalon fringes due to non-uniform transmission through optical windows, lens [64]. This appear as oscillations in $2f$ signals. The transmittance of laser through two windows with the distance between the windows as L is given by:

$$T = 1 - R = \frac{1}{1 + F \sin^2\left(\frac{\delta}{2}\right)} \quad (11)$$

Where F is the coefficient of finesse, given as, $F = \frac{4R}{(1-R)^2}$ and $\delta = \frac{2\pi}{\lambda} nL \cos \theta$. Here R is the reflectance of the optical components. For Mid-IR applications, ZnSe windows are usually used which has $T = 0.7$ for 2.0–14 μm region.

The Normalized Noise Equivalent Absorbance (NNEA) is calculated using Eq. (12):

$$NNEA = \alpha_{min} P \sqrt{t} \quad (12)$$

In the above equation α_{min} is the noise equivalent absorption coefficient (cm^{-1}), P is the incident optical power (W) and t is the measured time (s).

A summary of optical techniques and their normalized noise equivalent absorbance is given in **Table 4**.

3.2 Repeatability and Allan variance

Another important source of measurement error in spectroscopic systems is the repeatability of the measurement process. In trace level measurement, integration

Measurement technique	NNEA ($\text{Wcm}^{-1} \text{Hz}^{-1/2}$)	Spectral region (cm^{-1})	Ref.
Open path tunable diode laser absorption spectroscopy	6.32×10^{-8}	3778–3780	[65]
	6×10^{-9} – 8.419×10^{-11}	1246–1250	[66]
Cavity ring down spectroscopy	2.0×10^{-13}	9397–9399	[67]
	4.25×10^{-14}	6135–6369	[68]
	3.0×10^{-16}	6350–6380	[69]
Cavity enhanced spectroscopy	2.0×10^{-15}	6472–6693	[70]
	6.0×10^{-14}	6490–6555	[71]
Tunable diode laser photo-acoustic spectroscopy	2.2×10^{-9}	6525–6529	[72]
	5.19×10^{-10}	4038.8–4039	[73]
	1.2×10^{-7}	2310–2313	[74]
	3.2×10^{-10}	2310–2313	[75]

NNEA: normalized noise equivalent absorbance.

Table 4.

Summary of optical techniques for trace gas concentration measurement using laser absorption in both near IR and Mid-IR spectral region and its normalized noise equivalent absorbance.

time of the measurement or time-binning is an important parameter that helps us to study the repeatability of the system when laser frequency stability is a factor (not the systematic errors). The bandwidth of the measurement system becomes critical when one tries to measure multiple trace gases in a single measurement system.

Allan variance is defined as [76]:

$$\sigma_y^2(\tau) = \frac{1}{2\tau^2} \langle (\Delta^2 x)^2 \rangle = \frac{1}{2} \langle (\Delta y)^2 \rangle \quad (13)$$

and the deviation is given as

$$\sigma_y(\tau) = \sqrt{\sigma_y^2(\tau)} \quad (14)$$

A good discussion on using of Allan deviation for calibration of laser absorption spectrometer using QCLs is given in Ref. [77] by Smith et al. Optimization of sampling rates plays a major role in enabling high sensitivity measurement of QCL-based laser absorption spectrometers.

4. Enablers for industrial application

Some of the challenges of using Quantum Cascade Lasers for industrial applications have already been highlighted in previous sections in a different context. Few those challenges along with some new ones will be discussed here to avoid the desultoriness.

4.1 Window materials

Some of the common window materials used for Mid-IR applications are Sapphire, Calcium Fluoride (CaF_2), Barium Fluoride (BaF_2), Magnesium Fluoride (MgF_2) and Zinc Selenide (ZnSe). The transmittance from un-coated wedged windows (wedge angle: 30 ± 10 arcmin) is shown in **Figure 7**.

Though CaF_2 and BaF_2 can transmit over a broad wavelength range (around 10–14 μm), it is not suitable for combustion or high temperature applications in

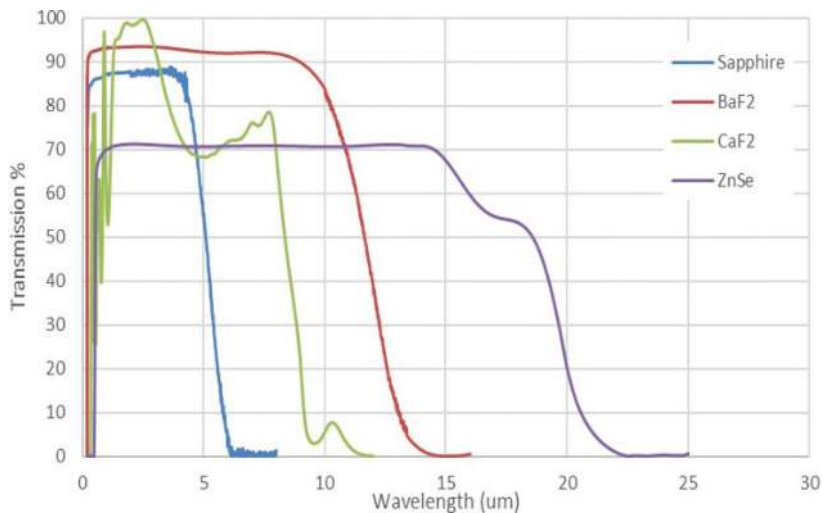


Figure 7. Transmission % from wedged windows of Sapphire, CaF_2 , BaF_2 and ZnSe with wavelength (μm). Data Source: Thorlabs catalog for optical windows [78].

presence of moisture. These materials are extremely hygroscopic and degrade in presence of moisture. Due to their large thermal expansion coefficients they are not suitable for combustion applications. ZnSe has much broader transmittance and has lower thermal expansion than the fluoride crystals. Sapphire is the most suitable material for high temperature and high-pressure combustion applications but it has a lower transmittance window compared to the Fluoride crystals and ZnSe (upto 4.0 μm). Careful selection of windows is required keeping in cognizant the following parameters: application conditions (temperature, pressure), gas species, etalon effects. A summary of the properties for the window materials is given in **Table 5**.

4.2 Optical fibers

It is always desirable in an industrial application to isolate the lasers from the operating environment to protect the lasers. Several types of fiber cables exist for delivery of Mid-IR laser beams. A summary of optical fibers available for Mid-IR range is given in **Table 6**.

The wavelength range covered by hollow core waveguides is widest among all the fibers available for Mid-IR laser beam transmission.

Window material	Refractive index range	Wavelength range (μm)	Thermal expansion coeff. ($1/^\circ\text{C}$)	Melting point ($^\circ\text{C}$)
SAPPHIRE	1.9–1.62	0.2–5.0	5.3×10^{-6}	1800
Calcium fluoride	1.58–1.3	0.2–10	18.85×10^{-6}	1418
Barium fluoride	1.65–1.3	0.2–15	18.4×10^{-6}	1368
Magnesium fluoride	1.43–1.3	0.2–6.7	13.7×10^{-6}	1255
Zinc selenide	2.75–2.35	0.5–16	7.1×10^{-6}	1520

Data Source: Thorlabs catalog for optical windows [78].

Table 5. Summary of optical and thermal properties of some common window materials used for Mid-IR applications.

Fiber type	Attenuation (dB/m)	Core diameter (μm)	Wavelength range (μm)	Ref
Zirconium (IV) fluoride	0.20	100, 200, 400	1.5–3.7	[79]
Zirconium (iv) fluoride	0.25	600	2.0–3.5	[79]
Indium (iii) fluoride	0.45	100	1.0–4.5	[79]
Hollow core waveguides	0.10	700	3.0–14	[17]
Hollow core waveguides	<1.0	300	7.6–11	[15]
Chalcogenide (as-s type)	0.12 (0.6)	100	2–3.5 (4.0)	[80]
Chalcogenide (As-se type)	0.2 (0.5)	100	2–8 (4.5)	[80]

Table 6. Mid-IR optical fibers with core diameters, attenuation and wavelength range.

4.3 Alignment of optics

For all practical applications, the laser beams need to remain in continuous alignment with the detector during all operational conditions. As discussed in Section 2.4, $1f$ -normalization of WMS- $2f$ is used to reject the background emissions (beam-steering, transmission losses due to dust particle scattering, window fouling) that vary much slowly with respect to $1f$. But for coarse alignment of the beam (due to thermal misalignment, etc.) one needs to use a different technique for automatic misalignment correction. In this case, a 633 nm laser is multiplexed with the Mid-IR lasers and transmitted through the gas flow path. The transmitted beam is demultiplexed and a quadrant photodetector is used as the position sensitive detector. The technique has been discussed in detail in Ref. [81] by Mitra et al.

4.4 Multi-wavelength detection

Simultaneous detection of multiple gases in combustion process is an unique challenge for a spectroscopy-based measurement. For example, one needs to measure NO, NO₂, CO, O₂ and H₂O simultaneously in the combustion gas mixture. This implies multiplexing of Mid-IR and Near-IR wavelengths for measurement. The demultiplexing process involves using CaF₂ (1–6 μm) or ZnSe (1–12 μm/7–14 μm) beam splitters to separate the Mid-IR and Near-IR beams [82].

Sequencing the laser operation and the detection is the key factor for the optimizing the sensor performance when we have multiple source and single detector. Mukherjee et al. [83] discussed about using scanning galvanometer to switch between the lasers (in <1 s) for multispecies trace gas detection. Time-division multiplexing (TDM) method has been reported by Dong et al. [84] where a stepper motor coupled to detectors were used for measurement of multiple gases.

For process control applications, the measurement time is usually between 1–10s. As highlighted in Section 3.2, optimization of integration time is required for each species to minimize the noise and drifts while carrying out all the measurements within the time window required for process control applications. A hybrid approach of wavelength and frequency multiplexing needs to be developed in accordance to the process requirement.

4.5 Calibration-free measurement

For all on-site measurements, periodic calibration of the measurement process is required for accurate estimation of concentration. Usually, a certified standard gas mixture in fiber-coupled gas cell is used for the calibration purpose [85]. A detailed calibration process steps have been discussed by Werle et al. in Ref. [86]. The “Zero” reading of the sensor is established using Nitrogen, Synthetic Air or local clean ambient air. Pre-mixed calibration gases of various concentrations are used for sensor “span” calibration. The “dynamic” calibration is finally carried out using a known test gas with the full sensor system in operational condition.

Presently most of the commercially available TDL-based sensors contains fiber coupled gas cells of high concentrations (also known as reference cell) of the target gas. A part of the laser beam is transmitted through the cell and used for line-locking of the transmitted beam. In this technique, a prudent selection of spectral region is required which is isolated from any neighboring transitions. Though in Mid-IR spectroscopy there is a good chance of locating these transitions, the implementation is quite challenging in applications which require trace level measurement in complex gas mixtures.

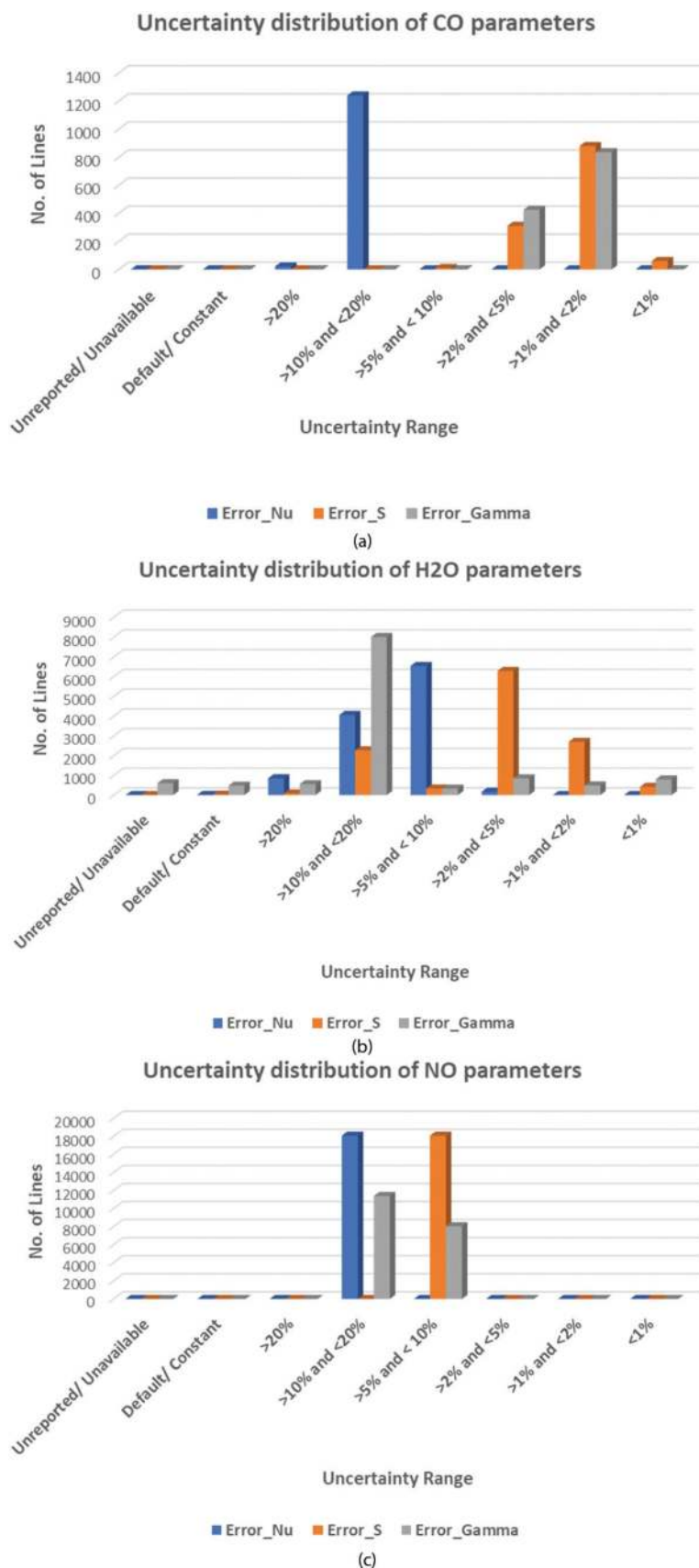


Figure 8. Uncertainty distribution of ν_0 , S and γ_{air} for (a) CO ($1900-2300\text{ cm}^{-1}$), (b) H₂O ($1500-2300\text{ cm}^{-1}$) and (c) NO ($1600-2200\text{ cm}^{-1}$).

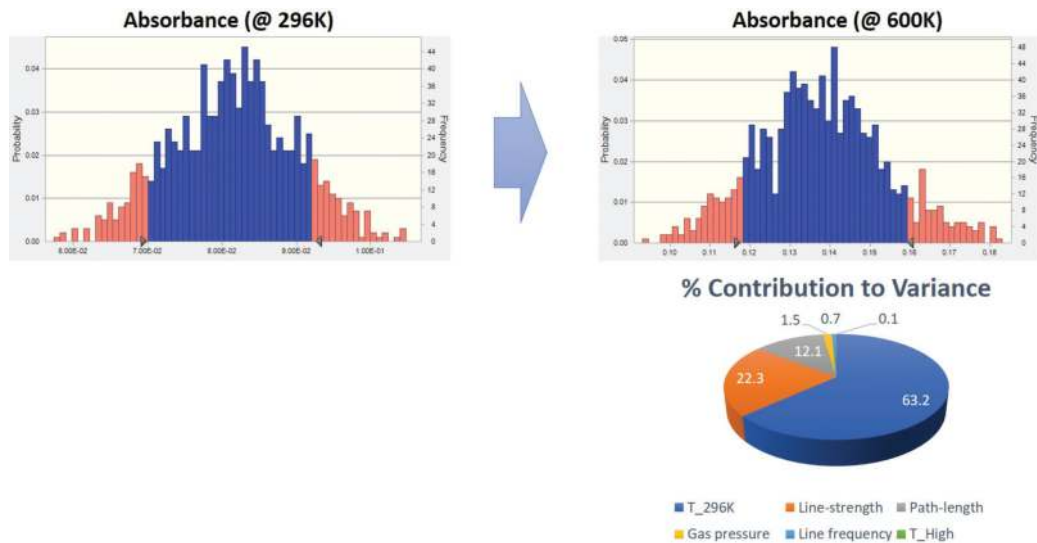


Figure 9.
 Monte-Carlo simulation of absorbance at 296 and 600 K with percentage contribution to variance.

There are broadly two versions of “Calibration-free” WMS technique reported in literatures. The first version discusses about using residual amplitude modulation (RAM) from the $1f$ signal for normalizing the incident laser intensity [87–89]. Like above, in this case too, the spectral region of interest should be well isolated from neighboring transitions. This limits the application in high gas pressure regime as the line broadening might blend the neighboring transitions. In addition to this, incident laser intensity fluctuations due to high vibrations, window fouling, beam steering are some of the major challenges for implementations of this technique.

In the second version of the “calibration free” technique, the WMS- $2f/1f$ signal obtained from actual measurement is compared against a model WMS- $2f/1f$ signal developed using laser tuning parameters and transition parameters used in the absorption feature under probe. The model is continuously updated based on the process parameters (T, P and gas concentration). A detailed explanation of the technique has been discussed by Rieker et al. and Sun et al. in Refs. [90, 91]. The same approach can be used for QCL-based measurements.

One of the major challenge with above method is the uncertainties with HITRAN spectral line parameters. **Figure 8** shows the uncertainty distributions for CO, NO and H₂O spectral parameters in the Mid-IR region [92].

It becomes a key to understand the impact of these uncertainties of the line parameters on absorbance and concentration estimation when measuring trace gas levels. Using the above details, a Monte-Carlo simulation was carried out to check the percentage contribution to variance at 600 K (**Figure 9**).

Figure 9 shows that in general the absorbance distribution (with 80% confidence interval) remains Gaussian at both 296 and 600 K temperatures. The major contribution for variance is due to variations from errors in measurement of temperature 296 K (63%) and uncertainties in line-strength (22%).

5. Conclusions

Since its discovery in 1994 by Capasso et al. [93], Quantum Cascade Lasers has come of age from being a laboratory tool to industrial application. It has opened the Mid-IR spectral region for industrial usage. Maturation of near-IR TDLAS

techniques over last 20 years and its applications using QCLs have opened a new vista for trace gas sensing for efficiency of combustion processes, environmental sensing for leak detection, emission and air quality monitoring. It also enabled explosives, chemicals and bio-hazard detection for law enforcement and defense agencies.

5.1 Takeaways

Availability of Mid-IR spectral region and improvements in WMS measurement scheme has enabled our ability to measure, CO, CO₂, NO, NO₂ accurately. Availability of High Heat Load (HHL) packages for QCLs, HCWs and robust detectors with multi-stage cooling, auto-alignment and calibration-free techniques has led to the application of QCLs in combustion process monitoring and controls.

5.2 Opportunities

Two broad categories of challenges remain to be addressed by Mid-IR spectroscopy.

First, the accuracy of spectroscopy databases in Mid-IR spectral region needs to be improved for high temperature applications. Only five species are covered in HITEMP (H₂O, CO, CO₂, NO, OH). High temperature parameters are based on quantum mechanical computations with uncertainties ranging from 5–20% and that limits the sensitivity of the measurement. Accurate HITEMP database is required for other combustion gases like NO₂, SO₂ and hydrocarbons.

Second, a major drawback with the Mid-IR fibers (HCWs) is their bending loss [17]. Also, the length of the HCWs available is not more than 1 m without significant transmission loss (<1 dB/m). For true remote application we need to have fibers >10 m. The Mid-IR lasers with improved performance and stability without additional cooling mechanisms are required for a robust sensor system.


Author details

Chayan Mitra

Environment Control Systems, Steam Power Systems, GE Power India Ltd.,
Noida, India

*Address all correspondence to: chayanmitra@yahoo.com

IntechOpen

© 2018 The Author(s). Licensee IntechOpen. This chapter is distributed under the terms of the Creative Commons Attribution License (<http://creativecommons.org/licenses/by/3.0>), which permits unrestricted use, distribution, and reproduction in any medium, provided the original work is properly cited. 

References

- [1] Purgert B, Shingledecker J. Update on U.S. DOE/OCDO advanced ultrasupercritical (A-USC) steam boiler and turbine consortium. EPRI, DOE-FE Cross-Cutting Review Meeting; 2015
- [2] GE Power. Powering the Future with Gas Power Systems: Offering 2018. USA: GEPower Offering; 2018
- [3] Wang J, Maiorov M, Baer DS, Garbuzov DZ, Connolly JC, Hanson RK. In-situ combustion measurements of CO with diode-laser absorption near $2.3\mu\text{m}$. *Applied Optics*. 2000;**39**(30): 5579-5589. DOI: 10.1364/AO.39.005579
- [4] Gmachl C, Capasso F, Sivco DL, Cho AY. Recent progress in quantum cascade lasers and applications. *Reports on Progress in Physics*. 2001;**64**(11):1533. DOI: 10.1088/0034-4885/64/11/204
- [5] Curl RF, Capasso F, Gmachl C, Kosterev AA, McManus B, Lewicki R, et al. Quantum cascade lasers in chemical physics. *Chemical Physics Letters*. 2010;**487**:1-18. DOI: 10.1016/j.cplett.2009.12.073
- [6] Wysocki G, Curl RF, Tittel FK, Maulini R, Bulliard JM, Faist J. Widely tunable mode-hop free external cavity quantum cascade laser for high resolution spectroscopic applications. *Applied Physics B*. 2005;**81**(6):769-777. DOI: 10.1007/s00340-005-1965-4
- [7] Meng B, Wang QJ. Broadly tunable single-mode mid-infrared quantum cascade lasers. *Journal of Optics*. 2015; **17**(2):023001. DOI: 10.1088/2040-8978/17/2/023001
- [8] Kosterev A, Wysocki G, Bakhrkin Y, So S, Lewicki R, Fraser M, et al. Application of quantum cascade lasers to trace gas analysis. *Applied Physics B: Lasers and Optics*. 2008;**90**:165-176. DOI: 10.1007/s00340-007-2846-9
- [9] Bismuto A, Blaser S, Terazzi R, Gresch T, Muller A. High performance, low dissipation quantum cascade lasers across the mid-IR range. *Optics Express*. 2015;**23**(5):5477-5484. DOI: 10.1364/OE.23.005477
- [10] VIGO Systems S.A. Catalogue; 2017
- [11] Piotrowski A, Piotrowski J, Gawron W, Pawluczyk J, Pedzinska M. Extension of usable spectral range of Peltier cooled photodetectors. *Acta Physica Polonica A*. 2009;**116**:S-52, S-55
- [12] Norton P. HgCdTe infrared detectors. *Opto-Electronics Review*. 2002;**10**(3):159-174
- [13] Krishnaswami K, Qiao H, Bernacki BE, Anheier N. Characterization of single-mode chalcogenide optical fiber for mid-infrared applications. *Proceedings of SPIE*. 2009;**7325**:73250Z. DOI: 10.1117/12.818184
- [14] Tao G, Abouraddy A. Advances in infrared fibers. *Proceedings of SPIE*. 2015;**9485**:94850K. DOI: 10.1117/12.2176403
- [15] Patimisco P, Sampaolo A, Mihai L, Giglio M, Kriesel J, Sporea D, et al. Low-loss coupling of quantum cascade lasers into hollow-core waveguides with single mode output in the $3.7\text{--}7.6\mu\text{m}$ spectral range. *Sensors*. 2016;**16**(533):1-11. DOI: 10.3390/s16040533
- [16] Sampaolo A, Patimisco P, Kriesel JM, Tittel FK, Scamarcio G, Spagnolo V. Single mode operation with mid-IR hollow fibers in the range $5.1\text{--}10.5\mu\text{m}$. *Optics Express*. 2015;**23**(1):195-204. DOI: 10.1364/OE.23.000195
- [17] Kriesel JM, Gat N, Bernacki BE, Erikson RL, Cannon BD, Myers TL, et al. Hollow Core Fiber optics for mid-wave and long-wave infrared

- spectroscopy. Proceedings of SPIE. 2011; 8018-8031. DOI: 10.1117/12.882840
- [18] Kriesel J, Gat N, Bernacki B, Myers T, Bledt C, Harrington J. Fiber Delivery of Mid-IR lasers. SPIE Newsroom (Defense & Security); 2011. DOI: 10.1117/2.1201108.003794
- [19] Harrington JA, Bledt CM, Kriesel JM. Hollow waveguides for the transmission of quantum cascade laser (QCL) energy for spectroscopic applications. Proceedings of SPIE. 2011; 7894:789414. DOI: 10.1117/12.881548
- [20] Patimisco P, Spagnolo V, Vitiello MS, Tredicucci A, Scamarcio G, Bledt CM, et al. Coupling external cavity mid-IR quantum cascade lasers with low loss hollow metallic/dielectric waveguides. Applied Physics B. 2012; 108(2):255-260. DOI: 10.1007/s00340-012-4891-2
- [21] Tittel FK, Richter D, Fried A. Mid-infrared laser applications in spectroscopy. Topics in Applied Physics: Solid State Mid-Infrared Laser Sources. 2003;89:445-516. DOI: 10.1007/3-540-36491-9
- [22] THORLABS. Reflective Optical Beam Expander. Product Catalogue
- [23] Sergchev I, Maulini R, Bismuto A, Blaser S, Gresch T, Bidaux Y, et al. All-electrical frequency noise reduction and linewidth narrowing in quantum cascade lasers. Optics Letters. 2014; 39(22):6411-6414. DOI: 10.1364/OL.39.006411
- [24] Gurel K, Schilt S, Bismuto A, Bidaux Y, Tardy C, Blaser S, Gresch T, Sudmeyer T. Characterization of a new frequency tuning and modulation mechanism for spectroscopy in a quantum cascade laser. OSA Technical Digest: CLEO. 2016; Applications of Semiconductor Lasers: Ath1J.2. DOI: 10.1364/CLEO_AT.2016.ATh1J.2
- [25] Gürell K, Schilt S, Bismuto A, Bidaux Y, Tardy C, Blaser S, et al. Frequency tuning and modulation of a quantum cascade laser with an integrated resistive heater. Photonics. 2016;3(3):47-59. DOI: 10.3390/photonics3030047
- [26] Nanoplus Nanosystems and Technologies GmbH. 5265.0nm DFB Laser. Product Specification; 2017
- [27] Bidaux Y, Bismuto A, Tardy C, Terazzi R, Gresch T, Blaser S, et al. Extended and quasi-continuous tuning of quantum cascade lasers using superstructure gratings and integrated heaters. Applied Physics Letters. 2015; 107(22):221108. DOI: 10.1063/1.4936931
- [28] Wavelength Electronics. QCL OEM Series QC Laser Driver. Product Datasheet and Operating Guide; 2016. pp. 1-23
- [29] Gordon IE, Rothman LS, Hill C, Kochanov RV, Tan Y, Bernath PF, et al. The HITRAN 2016 molecular spectroscopic database. Journal of Quantitative Spectroscopy and Radiative Transfer. 2017;203:3-69. DOI: 10.1016/j.jqsrt.2017.06.038
- [30] Rothman LS, Gordon IE, Barber RJ, Dothe H, Gamache RR, Goldman A, et al. HITEMP, the high temperature molecular spectroscopic database. Journal of Quantitative Spectroscopy and Radiative Transfer. 2010;111: 2139-2150. DOI: 10.1016/j.jqsrt.2010.05.001
- [31] Jacquinet-Husson N, Armante R, Scott NA, Chedin A, Crepeau L, Boutammime C, et al. The 2015 edition of the GEISA spectroscopic database. Journal of Molecular Spectroscopy. 2016;327:31-72. DOI: 10.1016/j.jms.2016.06.007
- [32] Sharpe SW, Johnson TJ, Sams RL, Chu PM, Rhoderick GC, Johnson PA. Gas-phase databases for quantitative

- infrared spectroscopy. *Applied Spectroscopy*. 2004;**58**(12):1452-1461. DOI: 10.1366/0003702042641281
- [33] Brown LR, Gunson MR, Toth RA, Irion FW, Rinsland CP, Goldman A. 1995 atmospheric trace molecule spectroscopy (ATMOS) linelist. *Applied Optics*. 1996;**35**(16):2828-2848. DOI: 10.1364/AO.35.002828
- [34] Chu PM, Guenther FR, Rhoderick GC, Lafferty WJ. The NIST quantitative infrared database. *Journal of Research of the National Institute of Standards and Technology*. 1999;**104**(1):59-81. DOI: 10.6028/jres.104.004
- [35] Barber RJ, Tennyson J, Harris GJ, Tolchenov RN. A high-accuracy computed water line list. *Monthly Notices of the Royal Astronomical Society*. 2006;**368**(3):1087-1094. DOI: 10.1111/j.1365-2966.2006.10184.x
- [36] Tashkun SA, Perevalov VI. CDSD-4000: High-resolution, high-temperature carbon dioxide spectroscopic databank. *Journal of Quantitative Spectroscopy and Radiative Transfer*. 2011;**112**(9):1403-1410. DOI: 10.1016/j.jqsrt.2011.03.005
- [37] Tennyson J, Bernath PF, Brown LR, Campargue A, Csaszar AG, Daumont L, et al. IUPAC critical evaluation of the rotational-vibrational spectra of water vapor, part III: Energy levels and transition wavenumbers for H₂(16)O. *Journal of Quantitative Spectroscopy and Radiative Transfer*. 2013;**117**:29-58. DOI: 10.1016/j.jqsrt.2012.10.002
- [38] Rothman LS, Gamache RR, Tipping RH, Rinsland CP, Smith MAH, Chris Benner D. The HITRAN molecular database: Editions of 1991 and 1992. *Journal of Quantitative Spectroscopy and Radiation Transfer*. 1992;**48**(5-6):469-507. DOI: 10.1016/0022-4073(92)90115-K
- [39] Rothman LS, Rinsland CP, Goldman A, Massie ST, Edwards DP, Flaud J-M. The HITRAN molecular spectroscopic database and HAWKS (HITRAN atmospheric workstation): 1996 edition. *Journal of Quantitative Spectroscopy and Radiative Transfer*. 1998;**60**(5):665-710. DOI: 10.1016/S0022-4073(98)00078-8
- [40] Goldman A, Brown LR, Schoenfeld WG, Spencer MN, Chackerian C Jr, Giver LP, et al. Nitric oxide line parameters: Review of 1996 HITRAN update and new results. *Journal of Quantitative Spectroscopy and Radiative Transfer*. 1998;**60**(5):825-838. DOI: 10.1016/S0022-4073(98)00085-5
- [41] Goldenstein CS, Miller VA, Spearrin RM, Strand CL. Spectra Plot.com: Integrated spectroscopic modeling of atomic and molecular gases. *Journal of Quantitative Spectroscopy & Radiative Transfer*. 2017;**200**:249-257. DOI: 10.1016/j.jqsrt.2017.06.007
- [42] Mitchell Spearrin R. Mid-infrared laser absorption spectroscopy for carbon oxides in harsh environments. Doctoral Thesis. Stanford University; 2014
- [43] Sur R. Development of robust TDLAS sensors for combustion products at high pressure and temperature in energy systems. Doctoral Thesis. Stanford University; 2014
- [44] Hanson RK, Spearrin RM, Goldenstein CS. *Spectroscopy and Optical Diagnostics for Gases*. 1st ed. USA: Springer; 2016. DOI: 10.1007/978-3-319-23252-2
- [45] Stancik AL, Brauns EB. A simple asymmetric lineshape for fitting infrared absorption spectra. *Vibrational Spectroscopy*. 2008;**47**(1):66-69. DOI: 10.1016/j.vibspec.2008.02.009
- [46] Belfhal A. The shape of spectral lines: Widths and equivalent widths of the Voigt profile. *Optic*

- Communication. 2000;**177**(1–6): 111-118. DOI: 10.1016/S0030-4018(00)00564-2
- [47] Tennyson J, Bernath PF, Campargue A, Csaszar AG, Daumont L, Gamache RR, et al. Recommended isolated-line profile for representing high-resolution spectroscopic transitions (IUPAC technical report). *Pure and Applied Chemistry*. 2014;**86**(12):1931-1943. DOI: 10.1515/pac-2014-0208
- [48] Vandeginste BGM, De Galan L. Critical evaluation of curve fitting in infrared spectrometry. *Analytical Chemistry*. 1975;**47**(13):2124-2132. DOI: 10.1021/ac60363a029
- [49] Draper NR, Smith H. *Applied Regression Analysis*. 3rd ed. John Wiley & Sons, Inc; 2014. 736 p. DOI: 10.1002/9781118625590
- [50] Birk M, Wagner G. Voigt profile introduces optical Stre depth dependent systematic errors – Detected in high resolution laboratory spectra of water. *Journal of Quantitative Spectroscopy and Radiative Transfer*. 2016;**170**: 159-168. DOI: 10.1016/j.jqsrt.2015.11.008
- [51] Claveau C, Henry A, Hurtmans D, Valentin A. Narrowing and broadening parameters of H₂O lines perturbed by He, Ne, Ar, Kr and nitrogen in the spectral range 1850-2140cm⁻¹. *Journal of Quantitative Spectroscopy and Radiative Transfer*. 2001;**68**(3):273-298. DOI: 10.1016/S0022-4073(00)00025-X
- [52] Varghese PL, Hanson RK. Collisional narrowing effects on spectral line shapes measured at high resolution. *Applied Optics*. 1984;**23**(14):2376-2385. DOI: 10.1364/AO.23.002376
- [53] Schultz I. Practical applications of laser absorption spectroscopy for aeroengine testing. Doctoral Thesis. Stanford University; 2014
- [54] Sur R, Peng WY, Strand C, Spearrin RM, Jefferies JB, Hanson RK, et al. Mid-infrared laser absorption spectroscopy of NO₂ at elevated temperatures. *Journal of Quantitative Spectroscopy and Radiative Transfer*. 2017;**187**: 364-374. DOI: 10.1016/j.jqsrt.2016.10.016
- [55] Rothman LS, Gordon IE, Babikov Y, Barbe A, Chris Benner D, Bernath PF, et al. The HITRAN 2012 molecular spectroscopic database. *Journal of Quantitative Spectroscopy and Radiative Transfer*. 2013;**130**:4-50. DOI: 10.1016/j.jqsrt.2013.07.002
- [56] Goorvitch D. Infrared CO line list for the X1 sigma (+) state. *The Astrophysical Journal Supplement Series*. 1994;**95**(2):535-552. DOI: 10.1086/192110
- [57] Spearrin RM, Ren W, Jeffries JB, Hanson RK. Multi-band infrared CO₂ absorption sensor for sensitive temperature and species measurements in high-temperature gases. *Applied Physics B*. 2014;**116**(4):855-865. DOI: 10.1007/s00340-014-5772-7
- [58] Zhou X, Liu X, Jeffries JB, Hanson RK. Development of a sensor for temperature and water concentration in combustion gases using a single tunable diode laser. *Measurement Science and Technology*. 2003;**14**(8):1459-1468. DOI: 10.1088/0957-0233/14/8/335
- [59] Sharma R, Mitra C, Tilak V. Diode laser-based trace detection of hydrogen-sulfide at 2646.3 nm and hydrocarbon spectral interference effects. *Optical Engineering*. 2016;**55**(3):037106-1-037106-6. DOI: 10.1117/1.OE.55.3.037106
- [60] Truong G-W, Anstie JD, May EF, Stace TM, Luiten AN. Accurate lineshape spectroscopy and the Boltzman constant. *Nature Communications*. 2015;**6**(8345):1-6. DOI: 10.1038/ncomms9345

- [61] Telle HH, Urena AG. *Laser Spectroscopy and Laser Imaging - an Introduction*. 1st ed. USA: CRC Press (Taylor & Francis Group); 2018
- [62] Sharma R, Mitra C, Maity S, Tilak V, Liu X, Kowal A, Tao C. System and Method for Measuring Concentration of a Trace Gas in a Gas Mixture. United States Patent Application Publication. 2017; US 2017/0003218 A1
- [63] Nagapriya KS, Sinha S, Prashanth R, Poonacha S, Chaudhry G, Bhattacharya A, et al. Laser calorimetry spectroscopy for ppm-level dissolved gas detection and analysis. *Scientific Reports*. 2017;7: 42917. DOI: 10.1038/srep42917
- [64] Cao J-n, Wang Z, Zhang K-k, Yang R, Wang Y. Etalon effects analysis in tunable diode laser absorption spectroscopy gas concentration detection system based on wavelength modulation spectroscopy. In: 2010 Symposium on Photonics and Optoelectronics (SOPO 2010) Proceedings; 19-21 June 2010; Chengdu, China. IEEE; 2010. DOI: 10.1109/SOPO.2010.5504036
- [65] Frish MB. Current and emerging laser sensors for greenhouse gas detection and monitoring. *Spectroscopy*. 2014;29(7)
- [66] Moser H, Polz W, Waclawek JP, Ofner J, Lendl B. Implementation of a quantum cascade laser-based gas sensor prototype for sub-ppmv H₂S measurements in a petrochemical process gas stream. *Analytical and Bioanalytical Chemistry*. 2017;409(3): 729-739. DOI: 10.1007/s00216-016-9923-z
- [67] Spence TG, Harb CC, Paldus BA, Zare RN, Willke B, Byer RL. A laser-locked cavity ring-down spectrometer employing an analog detection scheme. *The Review of Scientific Instruments*. 2000;71(2):347-353. DOI: 10.1063/1.1150206
- [68] Long DA, Truong G-W, van Zee RD, Plusquellic DF, Hodges JT. Frequency-agile, rapid scanning spectroscopy: Absorption sensitivity of 2×10^{-12} cm⁻¹ Hz^{-1/2} with a tunable diode laser. *Applied Physics B*. 2014;114(4):489-495. DOI: 10.1007/s00340-013-5548-5
- [69] Long DA, Fleisher AJ, Wójtewicz S, Hodges JT. Quantum-noise-limited cavity ring-down spectroscopy. *Applied Physics B*. 2014;115(2):149-153. DOI: 10.1007/s00340-014-5808-z
- [70] Axner O, Ehlers P, Foltynowicz A, Silander I, Wang J. NICE-OHMS—Frequency modulation cavity-enhanced spectroscopy—Principles and performance. In: Gagliardi G, Loock HP, editors. *Cavity-Enhanced Spectroscopy and Sensing*. Springer Series in Optical Sciences ed. Berlin, Heidelberg: Springer-Verlag; 2014. pp. 211-251. DOI: 10.1007/978-3-642-40003-2_6
- [71] Kasyutich VL, Sigrist MW. Characterisation of the potential of frequency modulation and optical feedback locking for cavity-enhanced absorption spectroscopy. *Applied Physics B*. 2013;111(3):341-349. DOI: 10.1007/s00340-013-5338-0
- [72] Webber ME, Pushkarsky M, Patel CKN. Fiber-amplifier-enhanced photoacoustic spectroscopy with near-infrared tunable diode lasers. *Applied Optics*. 2003;42(12):2119-2126. DOI: 10.1364/AO.42.002119
- [73] Tomberg T, Vainio M, Hieta T, Halonen L. Sub-parts-per-trillion level sensitivity in trace gas detection by cantilever-enhanced photoacoustic spectroscopy. *Scientific Reports*. 2018;8: 1848. DOI: 10.1038/s41598-018-20087-9
- [74] Kosterev AA, Bakhirkin YA, Curl RF, Tittel FK. Quartz-enhanced photoacoustic spectroscopy. *Optics Letters*. 2002;27(21):1902-1904. DOI: 10.1364/OL.27.001902

- [75] Patimisco P, Borri S, Scamarcio G, Spagnolo V, Galli I, Giusfedi G, et al. Cavity and quartz enhanced photoacoustic mid-IR sensor. In: Razeghi M, Tournié E, Brown GJ, editors. *Quantum Sensing and Nanophotonic Devices XI* (Proc. of SPIE - 8993). SPIE; 2014. pp. 899321-1-899321-8. DOI: 10.1117/12.2042246
- [76] Allan DW, Ashby N, Hodge CC. *The Science of Time-keeping*. Hewlett Packard Application Note 1289; 1997, USA. Hewlett-Packard Company Copyright © 1997 5965-7984E. pp. 1-88
- [77] Smith CJ, Wang W, Wysocki G. Real-time calibration of laser absorption spectrometer using spectral correlation performed with an in-line gas cell. *Optics Express*. 2013;**21**(19):22488-22503. DOI: 10.1364/OE.21.022488
- [78] THORLABS. *Optical Windows*. Product Catalogue
- [79] THORLABS. *Mid-Infrared Optical Fibers*. Product Catalogue
- [80] Lafond C, Couillard J-F, Delarosbil J-L, Sylvain F, de Sandro P. Recent improvements on mid-IR chalcogenide optical fibers. In: Andresen BF, Fulop GF, Hanson CM, Norton PR, editors. *Infrared Technology and Applications XL* (Proc. SPIE Vol. 9070). SPIE; 2014. p. 90701C (7 Pages). DOI: 10.1117/12.2050488
- [81] Mitra C, Sharma R. Diode laser-based sensor for extreme harsh environment data acquisition. In: Viskup R, editor. *High Energy and Short Pulse Lasers*. 1st ed. Croatia: InTech; 2016. pp. 393-415. DOI: 10.5772/63971
- [82] Mitra C, Joshi ND, Tilak V, Smith GR, Fung E, Sharma R, et al. *Gas Detector and Method of Detection*. United States Patent. 2016; US9500580B1
- [83] Mukherjee A, Prasanna M, Lane M, Go R, Dunayevskiy I, Tsekoun A, et al. Optically multiplexed multi-gas detection using quantum cascade laser photoacoustic spectroscopy. *Applied Optics*. 2008;**47**(27):4884-4887. DOI: 10.1364/AO.47.004884
- [84] Dong M, Zheng C, Miao S, Zhang Y, Du Q, Wang Y, et al. Development and measurements of a mid-infrared multi-gas sensor system for CO, CO₂ and CH₄ detection. *Sensors*. 2017;**17**(10): 2221-2235. DOI: 10.3390/s17102221
- [85] Swann WS, Gilbert SL. Accuracy limits for simple molecular absorption based wavelength references. In: Williams PA, Day GW, editors. *Symposium on Optical Fiber Measurements: Technical Digest*. NIST Special Publication 1024; 2004. pp. 15-17
- [86] Werle PW, Mazzinghi P, D'Amato F, De Rosa M, Maurer K, Slemr F. Signal processing and calibration procedures for in-situ diode laser absorption spectroscopy. *Spectrochimica Acta Part A*. 2004;**60**(8-9):1685-1705. DOI: 10.1016/j.saa.2003.10.013
- [87] Rieker GB. *Wavelength-modulation spectroscopy for measurements of gas temperature and concentration in harsh environments*. Doctoral Thesis. Stanford University; 2009
- [88] Duffin K, McGettrick AJ, Johnstone W, Stewart G, Moodie DG. Tunable diode-laser spectroscopy with wavelength modulation: A calibration-free approach to the recovery of absolute gas absorption line shapes. *Journal of Lightwave Technology*. 2007; **25**(10):3114-3125. DOI: 10.1109/JLT.2007.904937
- [89] McGettrick AJ, Duffin K, Johnstone W, Stewart G, Moodie DG. Tunable diode laser spectroscopy with wavelength modulation: A phasor

decomposition method for calibration-free measurements of gas concentration and pressure. *Journal of Lightwave Technology*. 2008;**26**(4):432-440. DOI: 10.1109/JLT.2007.912519

[90] Rieker GB, Jeffries JB, Hanson RK. Calibration-free wavelength-modulation spectroscopy for measurements of gas temperature and concentration in harsh environments. *Applied Optics*. 2009;**48**(29):5546-5560. DOI: 10.1364/AO.48.005546

[91] Sun K, Chao X, Sur R, Goldenstein CS, Jeffries JB, Hanson RK. Analysis of calibration-free wavelength-scanned wavelength modulation spectroscopy for practical gas sensing using tunable diode lasers. *Measurement Science and Technology*. 2013;**24**(12):125203-125215. DOI: 10.1088/0957-0233/24/12/125203

[92] Rothman LS, Jacquemart D, Barbe A, Benner DC, Birk M, Brown LR, et al. The HITRAN 2004 molecular spectroscopic database. *Journal of Quantitative Spectroscopy and Radiative Transfer*. 2005;**96**(2):139-204. DOI: 10.1016/j.jqsrt.2004.10.008

[93] Faist J, Capasso F, Sivco DL, Sirtori C, Hutchinson AL, Cho AY. Quantum cascade laser. *Science*. 1994;**264**(5158):553-556. DOI: 10.1126/science.264.5158.553